

Momentum correlations of the Hawking effect in a quantum fluid

Marcos Gil de Olivera,^{1,2} Malo Joly,¹ Antonio Z. Khouri,² Alberto Bramati,¹ and Maxime J. Jacquet^{1,*}

¹*Laboratoire Kastler Brossel, Sorbonne Université, CNRS,
ENS-Université PSL, Collège de France, Paris 75005, France*

²*Instituto de Física, Universidade Federal Fluminense, 24210-346 Niterói, RJ, Brazil*

(Dated: December 22, 2025)

The Hawking effect—the spontaneous emission of correlated quanta from horizons—can be observed in laboratory systems where an acoustic horizon forms when a fluid transitions from subcritical to supercritical flow. Although most theoretical and experimental studies have relied on real-space observables, the frequency-dependent nature of the Hawking process motivates a momentum-space analysis to access its spectral structure and entanglement features. Here, we numerically compute the momentum-space two-point correlation function in a quantum fluid using the truncated Wigner approximation, a general method applicable to both conservative and driven-dissipative systems. We consider a polaritonic fluid of light in a realistic configuration known to yield strong real-space correlations between Hawking, partner, and witness modes. We find signatures that are directly accessible in state-of-the-art experiments and offer a robust diagnostic of spontaneous emission. Our results form the basis for a new theoretical framework to assess a variety of effects, such as quasi-normal mode emission or modifications of the horizon structure on the Hawking spectrum.

The Hawking effect—the spontaneous emission of correlated pairs of field excitations from a horizon—is a fundamental prediction of quantum field theory in curved spacetime [1]. In quantum fluids of light or matter, an acoustic horizon forms when the flow transitions from subcritical to supercritical [2], allowing the emission of Hawking quanta [3], their negative-energy partner, and additional positive-energy witness modes due to superluminal dispersion. Although originally derived under relativistic assumptions [4, 5], this effect remains robust in dispersive media [6–8], and its frequency-dependent character is accessible via analog simulations of quantum field dynamics in curved spacetime [9].

Experimental implementations of these analog simulations have progressed rapidly [10]. In atomic BECs, the Hawking effect has been observed through real-space density-density correlations [11, 12], but full field measurements remain challenging. Photonic platforms, by contrast, enable direct access to non-commuting field quadratures—such as intensity and phase—offering in-situ full-field measurements in real time, along with tunable dispersion and engineered dissipation. Polaritonic fluids of light, in particular, offer unprecedented control: recent experiments have directly resolved individual horizon modes (including those with negative energy inside the horizon) on tunable curved spacetimes [13]. Control of the curvature and mode-resolution opens the door to investigating not only the Hawking effect itself but also its sensitivity to the near-horizon structure [14], including quasi-normal modes [15] and broadened/peaked horizon effects [16] as well as the interplay with rotational superradiance [17].

So far, signatures of the Hawking effect have often been identified via real-space density-density correlations, where paired emission yields interference features (“mustaches”) [18, 19]. However, these observables integrate over frequency, obscuring the spectral structure [20] and the entanglement content [21] of the emission. As the Hawking effect in analog simulators arises from scattering on a stationary background, momentum-space correlation functions are better

suited to characterize the output state. Analytical treatments in conservative systems have highlighted this advantage [22, 23], but no complete numerical study has addressed this in conservative or driven-dissipative platforms.

Here, we present the first numerical computation of momentum-space correlations in a transcritical quantum fluid. Our approach, based on the Truncated Wigner approximation, is broadly applicable to both dissipative and conservative systems in the regime of weak interactions and large occupation numbers, where quantum fluctuations remain perturbative. We apply this method to a polaritonic fluid of light in a previously identified optimal configuration for spontaneous Hawking emission [24]. The resulting spectra reveal clear, mode-resolved correlations in the output state, dominated by correlations across the horizon. This work establishes a general framework for analyzing the quantum state of horizon emission and provides experimentally relevant observables for entanglement diagnostics in quantum fluids of light or matter.

Collective excitations of a polaritonic fluid of light— We consider a quantum fluid of polaritons in a semiconductor microcavity etched into a wire along which the dynamics are purely one-dimensional, coherently driven near resonance by a continuous-wave laser. The mean-field dynamics of the polariton field $\psi(x, t)$ is governed by the driven-dissipative Gross-Pitaevskii equation (GPE) [25]

$$i\hbar \frac{\partial \psi(x, t)}{\partial t} = \left(\hbar\omega_0 - \frac{\hbar^2 \nabla^2}{2m^*} + \hbar g n(x, t) - i\hbar \frac{\gamma}{2} \right) \psi(x, t) + i\hbar \mathcal{F}(x, t), \quad (1)$$

where ω_0 is the frequency of polaritons at wavenumber $k = 0$, $\hbar^2 \nabla^2 \psi / 2m^*$ their kinetic energy in the cavity plane, and m^* their effective mass. $g > 0$ is the interaction strength and γ the loss rate. $\mathcal{F}(r, t) = F_p e^{i(k_p r - \omega_p t)}$ is the external coherent drive.

We first assume a spatially homogeneous configuration ($F_p, k_p = \text{cst}$). The field takes the form $\psi = \sqrt{n} e^{i(k_p x - \omega_p t)}$,

where $n = |\psi|^2$ is the polariton density. The steady-state density satisfies the nonlinear relation [26]

$$\left\{ [gn - \delta(k_p)]^2 + \frac{\gamma^2}{4} \right\} n = |F_p|^2, \quad (2)$$

whose solution depends on the frequency detuning $\delta(k_p) = \omega_p - \omega_0 - \hbar k_p^2 / 2m^*$.

To study collective excitations, we linearize the field around the steady state $\psi(x, t) = [\sqrt{n} + \varphi(x, t)e^{-\gamma t/2}]e^{i(k_p x - \omega_p t)}$ and expand $\varphi(x, t)$ in plane-wave modes as

$$\varphi(x, t) = \sum_q \left[u_q e^{i(qx - \omega t)} \hat{a}_q + v_q^* e^{-i(qx - \omega t)} \hat{a}_q^\dagger \right],$$

where q is the *relative* wave number with respect to the pump; the absolute momentum used below is $k = k_p + q$. u_q and v_q are complex mode functions, and $\hat{a}_q, \hat{a}_q^\dagger$ are bosonic annihilation and creation operators [27]. These obey the Bogoliubov-de Gennes equations in the driven-dissipative regime [25].

The Killing horizon— We now consider an inhomogeneous pump with structured wavevector $k_p(x)$ and intensity $|F_p(x)|^2$ in a one-dimensional wire, so that the stationary background density $n(x)$ and the flow velocity $v(x) = \hbar \partial_x(k_p(x)x)/m^*$ vary across a repulsive potential (height 0.85 meV and width 0.75 μm) centered at x_d . In practice, this may be achieved by local narrowing of the wire, creating a potential of a given width and depth [28]. As in [24], we use a steplike profile for the pump intensity and wavevector and a Gaussian potential for the defect [see the SM for technical details] and obtain a stationary mean field solution of (1). In the region $x - x_d < 0$, $\delta(k_p)$ is large enough to obtain a hysteresis cycle in Eq. (2). There, we choose $|F_p|^2$ so that gn is as close as possible to $\delta(k_p)$ [black dot in Fig. 1(a)], reaching the configuration found in [24] to maximize the correlations sought. In the region $x - x_d > 0$, $\delta(k_p)$ is small, so there is no hysteresis cycle. There, we choose $|F_p|^2$ to be high in the regime of nonlinear interactions, so as to have a finite density support in that region while minimizing density undulations induced by the phase mismatch between the two regions. We obtain the inhomogeneous profile shown in Fig. 1(b), where v (orange) is lower than the sound cone c_B (blue) for $x - x_d < 0$ and higher for $x - x_d > 0$. The density and velocity are homogeneous outside of the crossing region.

In the laboratory frame, the spectrum of collective excitations on either side of the horizon is [13]

$$\omega^\pm = vk \pm \sqrt{\left(\frac{\hbar k^2}{2m^*} - \delta(k_p) + 2gn \right)^2 - (gn)^2}. \quad (3)$$

The modes (u_q, v_q) corresponding to ω^+ have a positive symplectic norm $Q(|\varphi\rangle) = \int dx (|u_q|^2 - |v_q|^2)$, while ω^- have a negative norm [27].

The healing length $\xi = \sqrt{\hbar/m^*(2gn - \delta(k_p))}$ (evaluated in each asymptotic region) sets the microscopic scale over which density modulations relax and controls the low- $|q|$ Bogoliubov dispersion [27].

Figs. 1 (c) and (d) show the dispersion relation (3) in the regions $x - x_d < 0$ and $x - x_d > 0$. When v is small, the flow is subcritical and the positive- and negative-norm branches are at positive and negative frequencies, respectively. On the other hand, when v is large, the flow is supercritical: the ω^- branch is drawn to positive laboratory-frame frequencies (up to ω_{\max}) and, symmetrically, the ω^+ branch is drawn to negative laboratory-frame frequencies, allowing negative-energy modes ($\text{sign}(E) = \text{sign}(\omega) \times \text{sign}(Q)$ [29]) to be excited. This unambiguously signals the formation of a Killing horizon for collective excitations [13].

As we have $gn(x) \gtrsim \delta(k_p)(x)$ in both regions, the dispersion is parabolic even at low wavenumbers. In this case, the sound cones are not given by $c_s = \sqrt{\hbar gn/m^*}$ but by $c_B = \sqrt{\hbar(2gn - \delta(k_p))/m^*}$ [13]. φ is thus a field whose rest mass m_{det} is set by $|F_p|^2$ and $\delta(k_p)$, and which obeys a Klein-Gordon equation on a curved space-time, $\frac{1}{\sqrt{|g|}} \partial_\mu (\sqrt{|g|} g^{\mu\nu} \partial_\nu \varphi) - \frac{m_{\text{det}}^2}{\hbar^2} \varphi = 0$, where $v(x)$ and $c_B(x)$ define the Painlevé-Gullstrand line element $ds^2 = (c_B^2(x) - v^2(x)) dt^2 - 2v(x) dx dt + dx^2$ [30]. We denote the minimum frequency of the ω^+ branch upstream as ω_{\min} .

Hawking Effect— We now study the scattering of waves at the horizon. The system is stationary, so the frequency is conserved in the laboratory frame and the modes are found at the intersection between the dispersion (3) and an $\omega = \text{cst}$ line, see Fig. 1 (c) and (d). Given the dispersion on either side of the horizon, up and downstream, we can distinguish three regimes of propagation for the Bogoliubov excitations. Upstream, modes with positive group velocity $\partial\omega/\partial k$ propagate toward the horizon, while modes with negative group velocity propagate away from it, and conversely downstream. When $\omega < \omega_{\min}$, propagation is not allowed upstream while there are four propagating modes downstream. When $\omega_{\min} < \omega < \omega_{\max}$, there are two propagating modes upstream and four downstream. When $\omega > \omega_{\max}$, there are two propagating modes upstream and two downstream.

The Hawking effect results from the mixing of positive and negative energy modes on the horizon, resulting in Hawking radiation HR propagating upstream and its negative energy partner dn plus a positive-energy mode down (which represents the grey-body factor in the system [31]) downstream. Note that in quantum fluids with superluminal dispersion, the precursors of the Hawking effect originate from inside the horizon. As long as negative-energy modes are available and Hawking radiation can propagate away from the horizon upstream ($\omega_{\min} < \omega < \omega_{\max}$) this mixing is captured by the 3×3 scattering matrix [19]

$$\begin{pmatrix} \hat{b}_{\text{HR}} \\ \hat{b}_{\text{down}} \\ \hat{b}_{\text{dn}}^\dagger \end{pmatrix} = S_\omega \begin{pmatrix} \hat{a}_{\text{in}} \\ \hat{a}_p \\ \hat{a}_d^\dagger \end{pmatrix} \quad (4)$$

where the columns label, respectively, the incoming positive norm mode in, and the superluminal precursors of the positive norm p and negative norm d. The matrix elements encode both amplitude conversion and anomalous

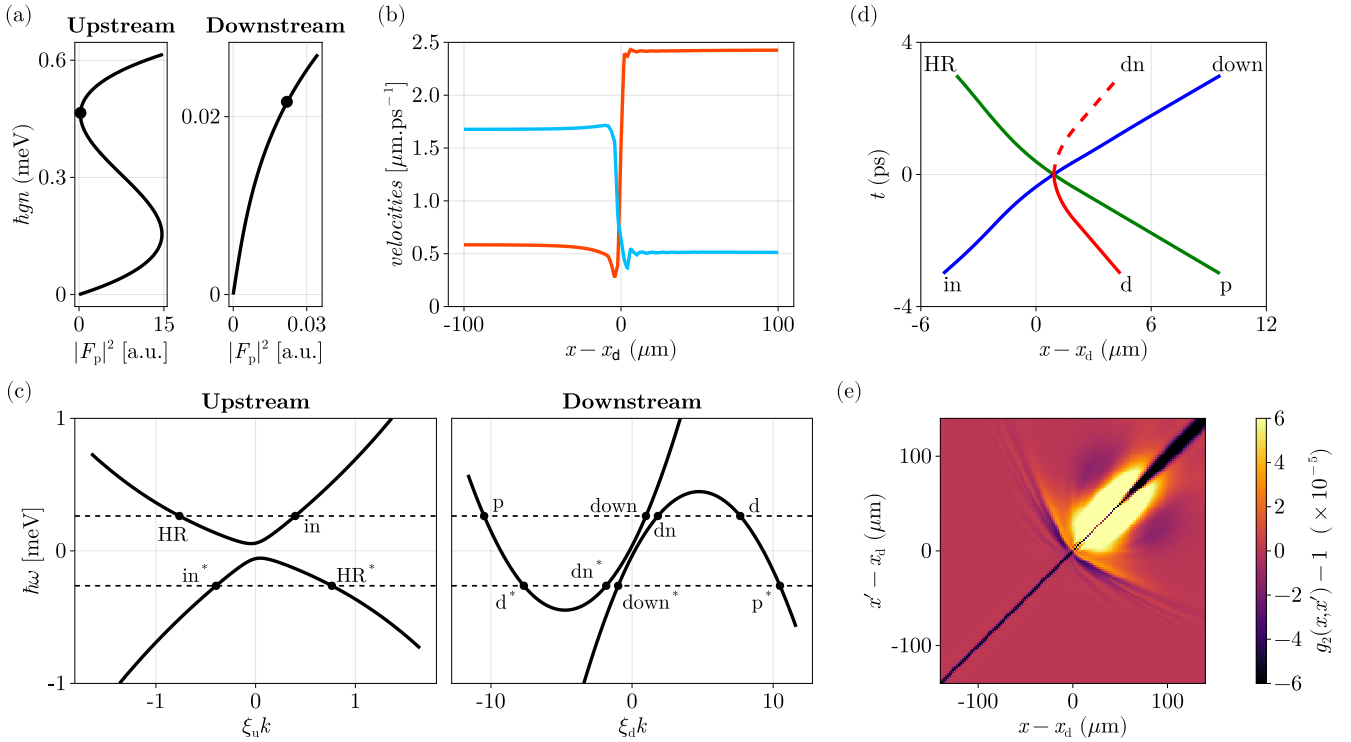


Figure 1. (a) Bistability curves Eq. (2). The dot denotes the working point. (b) Speed of fluid v (orange) and sound cones c_B (blue) as a function of position with origin at x_d . (c) Dispersion relation. (d) Trajectories according to a particle interpretation (WKB) of the scattering process at $\omega = 0.4 \text{ ps}^{-1}$. Blue, a regular mode that travels inwards; green, a lingering mode that eventually escapes as Hawking radiation (HR); red, the ‘turning mode’ of negative norm that becomes the partner (dn) in dashed. Together, HR and the dn represent the usual outgoing-ingoing relativistic particles (the would-be Hawking pairs) that peel infinitely at the horizon [14]. (e) Spatial density correlations $g_2(x, x') - 1$.

(Bogoliubov) mixing responsible for spontaneous pair creation. A complementary semi-classical picture is provided by the Wentzel–Kramers–Brillouin (WKB, that is, local density approximation) rays plotted in Fig. 1 (d): for a typical $\omega \in [\omega_{\min}, \omega_{\max}]$, the trajectories illustrate how the incoming modes fly out into the outgoing channels specified by S_ω [14].

The entries of the scattering matrix are calculated from the classical scattering problem and may be analytically expressed for some simple cases to calculate expectation values within the Bogoliubov theory [19]. In the present case, the profile is not integrable and fast (although small) variations in the mean-field properties plus the driven-dissipative dynamics render an analytical approach challenging. Instead, we used the truncated-Wigner approximation to numerically simulate the quantum dynamics of the polariton field $\hat{\psi}(x)$ in terms of averages over a stochastic process [see SM; the code used can be found in [32, 33]].

In the spatial configuration of Fig. 1 (b) (with a repulsive potential), the second-order spatial density-density correlation function $g_2(x, x') - 1 = \frac{\langle \hat{\psi}^\dagger(x') \hat{\psi}^\dagger(x) \hat{\psi}(x) \hat{\psi}(x') \rangle}{\langle \hat{\psi}^\dagger(x) \hat{\psi}(x) \rangle \langle \hat{\psi}^\dagger(x') \hat{\psi}(x') \rangle} - 1$ shown in Fig. 1 (e) features a ‘‘moustache’’ in the $xx' < 0$ region, signaling correlations between excitations propagating in opposite directions on either side of the horizon [18, 20, 34–36]. Now, one would want to distinguish Hawking-partner from

Hawking-witness correlation traces but, as in all quantum fluids, they spatially overlap due to dispersion. So, a momentum-space analysis is needed to analyse the output state [15].

Pairing structure in momentum space— The scattering process at the horizon imprints correlations among the outgoing Bogoliubov modes. From the structure of Eq. (4), we see that the outgoing operators \hat{b}_{HR} , \hat{b}_{down} , $\hat{b}_{\text{dn}}^\dagger$ are linear combinations of the incoming operators, including the conjugate of \hat{a}_d due to norm mixing. Consequently, the final quantum state exhibits both diagonal terms—occupation numbers such as $\langle \hat{b}_i^\dagger \hat{b}_i \rangle$ —and off-diagonal two-mode correlations of the form $\langle \hat{b}_i \hat{b}_j \rangle$, reflecting spontaneous pair creation.

Within Bogoliubov theory, the quantum field operator contains both annihilation and creation operators. For modes of negative norm such as dn, the relevant operator appearing in observables is b_{dn} , not its Hermitian conjugate, because of the anomalous sign in the commutation relations. This implies that the dominant pair correlation is anomalous: $\langle b_{\text{HR}} b_{\text{dn}} \rangle \neq 0$. This structure arises universally in the creation of horizon-induced pairs and is the direct signature of the spontaneous Hawking effect. It leads to a violation of the Cauchy–Schwarz inequality [22, 23, 37], indicating the non-separability of the outgoing state and confirming its quantum character. In contrast, correlations such as $\langle b_{\text{HR}} b_{\text{dn}}^\dagger \rangle$, though

allowed by symmetry, are generically suppressed unless induced by temperature or nonadiabatic effects. In summary, the Hawking-partner correlations we seek are $\text{HR} - \text{dn}^*$.

Analytical predictions for the two-body correlation function $g_2(k, k')$ are that the $\text{HR}-\text{dn}^*$ channel dominates the signal and survives far beyond the regime in which the thermal occupation numbers obscure the diagonal terms [12, 22, 23, 37]. These correlations are predicted to be enhanced at low frequencies, peak near ω_{\min} , and decay as $\omega \rightarrow \omega_{\max}$, reflecting the frequency dependence of the underlying Bogoliubov coefficients [16, 38].

To identify the various correlation lines in a momentum-momentum plot $g_2(k, k')$, one tracks the dispersion relation of the corresponding outgoing modes. At fixed frequency ω , the allowed momenta k in each asymptotic region are given by the Bogoliubov dispersion (3). For each outgoing mode (e.g. HR, down, dn), this equation defines a locus $k_i(\omega)$. These solutions are real within the frequency window of the horizon $\omega_{\min} < \omega < \omega_{\max}$, and the sign of the Bogoliubov norm distinguishes between positive- and negative-energy branches.

In Fig. 2 we calculate the correlations

$$\delta g_2 \equiv g_2(k, k') - 1 = \frac{\langle \hat{\psi}_u^\dagger(k') \hat{\psi}_d^\dagger(k) \hat{\psi}_d(k) \hat{\psi}_u(k') \rangle}{\langle \hat{\psi}_d^\dagger(k) \hat{\psi}_d(k) \rangle \langle \hat{\psi}_u^\dagger(k') \hat{\psi}_u(k') \rangle} - 1 \quad (5)$$

for two window configurations. In configuration (a), the windows are equal and centred at the horizon, while in configuration (b), they are centered on either side of the horizon, giving the correlation maps (c) and (d), respectively [see the SM for numerical parameters].

Quantum correlations— When both windows fully overlap (Fig. 2 (a)), the correlations in Fig. 2 (c) show a symmetric pattern (i)-(ii)-(iii) with respect to the exchange of k and k' . This exchange symmetry holds only for equal windows; it should not be interpreted as a $q \leftrightarrow q'$ symmetry. In our convention $k = k_p + q$, and because a Bogoliubov mode at $+q$ contains field components at $\pm q$ with unequal weights $u_q \neq v_q$, one generally has $\delta g_2(k_p + q, k') \neq \delta g_2(k_p - q, k')$. This symmetry arises because the overlap of the windows over the horizon leads to correlations between modes on the same side of the horizon.

Now, with the window configuration of Fig. 2 (b), the situation is quite different. Because the two Hann windows are identical but placed on opposite sides of the horizon, their cross-convolution cancels the large self-overlap terms, thereby suppressing autocorrelations and allowing the off-diagonal $\text{HR}-\text{dn}^*$ signal to emerge prominently. Fig. 2 (d) clearly illustrates how the separation of the windows has suppressed both the diagonal (i) and the anti-diagonal (ii)-(iii) traces at short k . Furthermore, we observe bands of zero correlation that run along the lines $k = k_{\text{down}}$, $k' = k_{\text{up}}$. These are due to spectral leakage of the pump modes which are amplified by the windows. We observe that the correlations are no longer symmetric around the diagonal and the Hawking traces are clearly visible starting from the region around $k = k_{\text{down}}$,

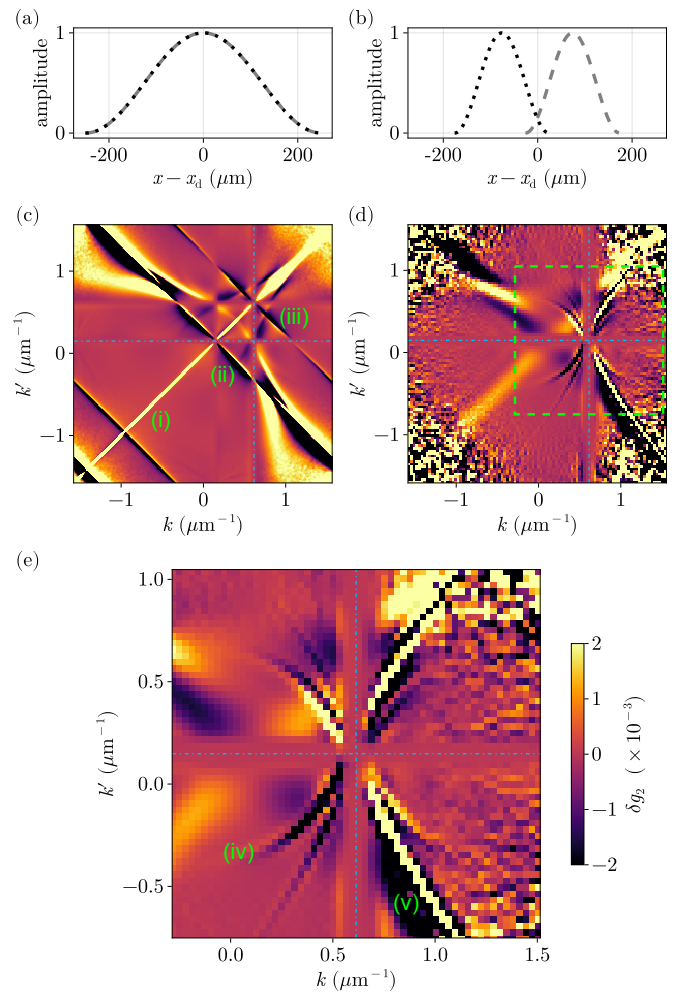


Figure 2. (a) Equal size windows centred at the horizon. (b) Equal size windows on opposite sides of the horizon. (c) Momentum density correlations (5) for the window functions in (a). (d) Momentum density correlations (5) for the window functions in (b). (e) Enlarged view of (d) in the region containing the correlations between modes on opposite sides of the horizon. Dot-dashed lines, k_{up} , k_{down} .

$k' = k_{\text{up}}$ and all the way to k values corresponding to ω_{\max} for each mode pair, crossing the diagonal and anti-diagonal in places. In the SM, we discuss the separation of the windows on either side of the horizon and its influence on the correlation strength and on the noise amplitude. In particular, we find that increasing the distance between the windows and the horizon decreases the correlations and increases the noise, which is due to the limited polariton lifetime and contrasts with results in closed systems [23].

Fig. 2 (e) zooms on the region dominated by the Hawking correlations. Two families of cross-horizon traces are visible: (iv), $\text{HR}-\text{dn}^*$ (the anomalous Hawking-partner channel); and (v), $\text{HR}-\text{down}$ (the grey-body channel). With identical windows [panel (c)], $\delta g_2(k, k')$ is symmetric under exchange of its arguments, $\delta g_2(k, k') = \delta g_2(k', k)$. With separated windows [panels (d-e)] this exchange symmetry is no longer expected; however the global sign-reversal $(q, q') \mapsto (-q, -q')$

remains exact. Consequently, each physical trace (HR–dn* or HR–down) appears in four quadrants related by this sign symmetry, yielding eight traces in total. These symmetries are enforced by the real nature of the field operator and the bosonic commutation relations and serve as consistency checks [23, 38].

Although each trace has a well-defined sign when the windows overlap on the horizon [Fig. 2 (c)], with a positive correlation when both modes have the same sign of $\omega - \omega_p$ and a negative correlation when they have the opposite sign of $\omega - \omega_p$, this is not the case when the windows are separated around the horizon. In Fig. 2 (e) we see that all traces have mixed, or coexisting, correlation signs, which is typical of an interferometric Fano-like response. This is likely due to the interplay between the finite-window support and the fast and extreme variation of the mean-field properties across the horizon. Notably, the HR–dn* trace is dominated by negative correlations, a signature of their quantum vacuum origin and of the non-separability of the involved excitation modes [23]. Overall, all important features have $|\delta g_2| \geq 10^{-3}$.

Discussion— In this work, we have numerically calculated the momentum density correlations stemming from the Hawking effect at a horizon in a quantum fluid. We observed sharp correlation traces between Hawking radiation and its partner wave, as well as with the so-called witness mode characteristic of superluminal dispersions. In doing so, we have confirmed and complemented analytical calculations in simpler configurations in closed systems [22, 23].

Our methods are readily generalizable to other one-dimensional systems such as flowing atomic BECs or other configurations in which near-horizon variations of the mean field have been found to leave an imprint on the Hawking spectrum [15, 36]. They could also be applied to rotating two-dimensional geometries [39, 40], opening the way to a frequency-resolved study of the amplification of vacuum fluctuations with and without horizons and to study analytical predictions on entanglement generation [41].

Finally, for the parameters of Fig. 2, the peak-normalized Hawking correlation reaches $|\delta g_2| \sim 10^{-3}$ in the HR–dn* channel. In the laboratory, this can be accessed by selecting the two corresponding far-field momentum windows and measuring the zero-delay cross-covariance of the associated photocurrents (or, equivalently, the deviation of the balanced-difference noise power from the shot-noise level in a balanced receiver). In the shot-noise-limited regime, the signal-to-noise of this covariance estimate scales as $\propto \sqrt{BT}$, where B is the electronic bandwidth and T the integration time. Operating in the MHz regime with $B \simeq 10$ MHz and collecting a photon flux per window $\sim 10^{13} \text{ s}^{-1}$ (corresponding to $10 \mu\text{W}$ -level powers at ~ 830 nm [13] and μA -level photocurrents), one has $\sqrt{BT} \approx 2.5 \times 10^4$ for $T = 1$ min, so that correlations at the 10^{-3} level are detectable with minute-scale acquisitions up to order-unity prefactors. The exact acquisition time depends on the achieved common-mode rejection of residual classical noise and on the detector quantum efficiency [see SM]. These considerations indicate that the Hawking cor-

relations reported here are within reach of current balanced-detection and far-field correlation measurements.

ACKNOWLEDGEMENTS

We are thankful to Kévin Falque, Killian Guerrero, Iacopo Carusotto, and Nicolas Pavloff for their insights on polaritons and the Hawking effect. The authors also thank Killian Guerrero for feedback on the manuscript. MJJ and AB acknowledge funding from the EU Pathfinder 101115575 Q-One. AB acknowledges support from the Institut Universitaire de France. MGO acknowledges the sponsorship by Coordenação de Aperfeiçoamento de Pessoal do Ensino Superior - CAPES of his six-month internship at Laboratoire Kastler Brossel - LKB. AZK acknowledges support from Conselho Nacional de Desenvolvimento Científico e Tecnológico (CNPq 422300/20217); Fundação Carlos Chagas Filho de Amparo à Pesquisa do Estado do Rio de Janeiro (FAPERJ).

* maximjacquet@gmail.com

- [1] R. M. Wald, *Quantum Field Theory in Curved Space-Time and Black Hole Thermodynamics*, Chicago Lectures in Physics (University of Chicago Press, Chicago, IL, 1995).
- [2] M. Visser, Acoustic black holes: horizons, ergospheres and Hawking radiation, *Classical and Quantum Gravity* **15**, 1767 (1998).
- [3] W. G. Unruh, Experimental black-hole evaporation?, *Physical Review Letters* **46**, 1351 (1981).
- [4] S. W. Hawking, Black hole explosions?, *Nature* **248**, 30 (1974).
- [5] R. M. Wald, On particle creation by black holes, *Communications in Mathematical Physics* **45**, 9 (1975).
- [6] R. Brout, S. Massar, R. Parentani, and P. Spindel, Hawking radiation without trans-Planckian frequencies, *Physical Review D* **52**, 4559 (1995).
- [7] W. G. Unruh, Sonic analogue of black holes and the effects of high frequencies on black hole evaporation, *Physical Review D* **51**, 2827 (1995).
- [8] S. Corley and T. Jacobson, Hawking spectrum and high frequency dispersion, *Physical Review D* **54**, 1568 (1996).
- [9] C. Barceló, S. Liberati, and M. Visser, *Analogue Gravity*, *Living Reviews in Relativity* **14**, 3 (2011).
- [10] C. R. Almeida and Jacquet, Maxime J., Analogue gravity and the Hawking effect: historical perspective and literature review, *Eur. Phys. J. H History for Physics: Contextualizing Modern Developments in the Foundations of Quantum Theory*, **48**, 15 (2023).
- [11] J. R. Muñoz de Nova, K. Golubkov, V. I. Kolobov, and J. Steinbauer, Observation of thermal Hawking radiation and its temperature in an analogue black hole, *Nature* **569**, 688 (2019).
- [12] M. Isoard and N. Pavloff, Departing from Thermality of Analogue Hawking Radiation in a Bose-Einstein Condensate, *Physical Review Letters* **124**, 060401 (2020).
- [13] K. Falque, A. Delhom, Q. Glorieux, E. Giacobino, A. Bramati, and M. J. Jacquet, Polariton Fluids as Quantum Field Theory Simulators on Tailored Curved Spacetimes, *Physical Review Letters* **135**, 10.1103/1538-0606/135/101103 (2025).

[14] F. Del Porro, S. Liberati, and M. Schneider, Tunneling method for Hawking quanta in analogue gravity, *Comptes Rendus. Physique* **25**, 1 (2024).

[15] M. Jacquet, L. Giacomelli, Q. Valnais, M. Joly, F. Claude, E. Giacobino, Q. Glorieux, I. Carusotto, and A. Bramati, Quantum Vacuum Excitation of a Quasinormal Mode in an Analog Model of Black Hole Spacetime, *Physical Review Letters* **130**, 111501 (2023).

[16] S. Finazzi and R. Parentani, Spectral properties of acoustic black hole radiation: Broadening the horizon, *Physical Review D* **83**, 084010 (2011).

[17] I. Agullo, A. J. Brady, A. Delhom, and D. Kranas, Entanglement from rotating black holes in thermal baths, *Phys. Rev. D* **110**, 025021 (2024).

[18] I. Carusotto, S. Fagnocchi, A. Recati, R. Balbinot, and A. Fabbri, Numerical observation of Hawking radiation from acoustic black holes in atomic Bose-Einstein condensates, *New Journal of Physics* **10**, 103001 (2008).

[19] A. Recati, N. Pavloff, and I. Carusotto, Bogoliubov theory of acoustic hawking radiation in bose-einstein condensates, *Phys. Rev. A* **80**, 043603 (2009).

[20] R. Balbinot, A. Fabbri, S. Fagnocchi, A. Recati, and I. Carusotto, Nonlocal density correlations as a signature of Hawking radiation from acoustic black holes, *Physical Review A* **78**, 021603 (2008).

[21] M. Isoard, N. Milazzo, N. Pavloff, and O. Giraud, Bipartite and tripartite entanglement in a bose-einstein acoustic black hole, *Phys. Rev. A* **104**, 063302 (2021).

[22] D. Boiron, A. Fabbri, P.-E. Larré, N. Pavloff, C. I. Westbrook, and P. Zií, Quantum signature of analog hawking radiation in momentum space, *Physical Review Letters* **115**, 025301 (2015).

[23] A. Fabbri and N. Pavloff, Momentum correlations as signature of sonic Hawking radiation in Bose-Einstein condensates, *SciPost Physics* **4**, 019 (2018).

[24] M. Jacquet, M. Joly, F. Claude, L. Giacomelli, Q. Glorieux, A. Bramati, I. Carusotto, and E. Giacobino, Analogue quantum simulation of the Hawking effect in a polariton superfluid, *The European Physical Journal D* **76**, 152 (2022).

[25] M. J. Jacquet, *Superradiant amplification: experimental and theoretical study in a polaritonic fluid of light*, Accreditation to supervise research, Sorbonne Université (2025).

[26] A. Baas, J. P. Karr, H. Eleuch, and E. Giacobino, Optical bistability in semiconductor microcavities, *Phys. Rev. A* **69**, 023809 (2004).

[27] Y. Castin, Bose-einstein condensates in atomic gases: Simple theoretical results, in *Coherent atomic matter waves*, edited by R. Kaiser, C. Westbrook, and F. David (Springer Berlin Heidelberg, Berlin, Heidelberg, 2001) pp. 1–136.

[28] H. S. Nguyen, D. Gerace, I. Carusotto, D. Sanvitto, E. Galopin, A. Lemaître, I. Sagnes, J. Bloch, and A. Amo, Acoustic black hole in a stationary hydrodynamic flow of microcavity polaritons, *Physical Review Letters* **114**, 036402 (2015).

[29] N. N. Bogoliubov, On the theory of superfluidity, *J. Phys. (USSR)* **11**, 23 (1947).

[30] The polariton lifetime in our microcavity is $\tau \approx 15$ ps. The correlations are sampled over $\lesssim 3\tau$, during which the mean-field profile remains locked by the CW pump. The weak Hawking flux therefore produces no measurable back-reaction, so the Killing horizon serves as the relevant event horizon for Bogoliubov modes.

[31] I. Agullo, A. J. Brady, and D. Kranas, Event horizons are tunable factories of quantum entanglement, *International Journal of Modern Physics D* **31**, 2242008 (2022).

[32] M. Gil de Oliveira, *GeneralizedGrossPitaevskii.jl* (2025).

[33] M. Gil de Oliveira, *momentum.correlation.polaritons* (2025).

[34] D. Gerace and I. Carusotto, Analog hawking radiation from an acoustic black hole in a flowing polariton superfluid, *Physical Review B* **86**, 144505 (2012).

[35] P. Grišins, H. S. Nguyen, J. Bloch, A. Amo, and I. Carusotto, Theoretical study of stimulated and spontaneous hawking effects from an acoustic black hole in a hydrodynamically flowing fluid of light, *Physical Review B* **94**, 144518 (2016).

[36] M. Burkhard, M. Kroi, K. Falque, A. Bramati, I. Carusotto, and M. J. Jacquet, Stimulated hawking effect and quasinormal mode resonance in a polariton simulator of field theory on curved spacetime, *arXiv:2511.12339* (2025).

[37] X. Busch and R. Parentani, Quantum entanglement in analogue hawking radiation: When is the final state nonseparable?, *Physical Review D* **89**, 105024 (2014).

[38] J. Macher and R. Parentani, Black/white hole radiation from dispersive theories, *Physical Review D* **79**, 124008 (2009).

[39] P. Švančara, P. Smaniotti, L. Solidoro, J. F. MacDonald, S. Patrick, R. Gregory, C. F. Barenghi, and S. Weinfurtner, Rotating curved spacetime signatures from a giant quantum vortex, *Nature* **628**, 66 (2024).

[40] K. Guerrero, K. Falque, E. Giacobino, A. Bramati, and M. J. Jacquet, Multiply quantized vortex spectroscopy in a quantum fluid of light, *Phys. Rev. Lett.* **135**, 243801 (2025).

[41] A. Delhom, K. Guerrero, P. Calizaya Cabrera, K. Falque, A. Bramati, A. J. Brady, M. J. Jacquet, and I. Agullo, Entanglement from superradiance and rotating quantum fluids of light, *Physical Review D* **109**, 105024 (2024).

Supplemental Material

Marcos Gil de Olivera,^{1,2} Malo Joly,² Antonio Z. Khouri,¹ Alberto Bramati,² and Maxime J. Jacquet^{2,*}

¹*Instituto de Física, Universidade Federal Fluminense, 24210-346 Niterói, RJ, Brazil*

²*Laboratoire Kastler Brossel, Sorbonne Université, CNRS,
ENS-Université PSL, Collège de France, Paris 75005, France*

(Dated: December 22, 2025)

POLARITON KINEMATICS

Polaritons are quasiparticles of mass m^* resulting from the strong coupling of cavity photons and quantum well excitons. Under coherent excitation by a pump $F(x, t)$ near resonance with the cavity, the mean field of polaritons can be described by the driven dissipative Gross-Pitaevskii equation [1]

$$i\partial_t\psi(x, t) = F(x, t) + \left(\omega_0 - \frac{i\gamma}{2} - \frac{\hbar\partial_x^2}{2m^*} + g|\psi(x, t)|^2 + V(x)\right)\psi(x, t). \quad (1)$$

ω_0 is the polariton frequency at wavenumber $k = 0$, γ the (mostly photonic) decay rate, $g > 0$ the repulsive interaction strength and $V(x)$ the potential reigning in the cavity.

We consider a monochromatic pump $F(x, t) = F(x)e^{-i\omega_p t}$. Then, it is useful to decompose the polariton field as $\psi(x, t) = \sqrt{n(x, t)}e^{i(\theta(x, t) - \omega_p t)}$. The density n and the phase θ satisfy the equations

$$\partial_t n + \partial_x(nv) = -\gamma n + 2\sqrt{n} \operatorname{Im} Fe^{-i\theta}; \quad (2)$$

$$\partial_t\theta + gn - \delta_0 + \frac{m^*v^2}{2\hbar} + V - \frac{\hbar}{2m^*} \frac{\partial_x^2 \sqrt{n}}{\sqrt{n}} + \frac{\operatorname{Re} Fe^{-i\theta}}{\sqrt{n}} = 0. \quad (3)$$

We have defined the velocity of the fluid as $v = \hbar\partial_x\theta/m^*$ and the bare detuning $\delta_0 = \omega_p - \omega_0$. Eq. (2) is the continuity equation, while the gradient of Eq. (3) is analogous to the Euler equation.

When considering plane wave pump of the form $F(x) = \sqrt{I}e^{ik_p x}$, we may seek a stationary ($\partial_t n = \partial_t\theta = 0$) and homogeneous ($\partial_x n = \partial_x v = 0$) solution of (2) and (3). By writing $\theta(x) = k_p x + \theta_0$, we conclude that

$$0 = -\gamma n - 2\sqrt{nI} \sin\theta_0; \quad (4)$$

$$gn - \delta + \sqrt{\frac{I}{n}} \cos\theta_0 = 0. \quad (5)$$

where we have introduced the detuning $\delta = \delta_0 - \frac{\hbar k_p^2}{2m} + V$. Then, we arrive at the solutions

$$\left[(gn - \delta)^2 + \frac{\gamma^2}{4} \right] n = I, \quad (6)$$

$$\theta_0 = \arctan \left[\frac{\gamma}{2(\delta - gn)} \right] \quad (7)$$

THE TRUNCATED WIGNER APPROXIMATION

The Truncated Wigner Method (TWM) allows one to efficiently simulate quantum expectation values and has been extensively employed in studies of polaritons [2]. The master equation for this system in the Wigner representation may be approximated by a Fokker-Planck equation if the condition $\gamma \ll g/\Delta x$ is satisfied, where Δx is the grid spacing used in the simulation. The corresponding Langevin equations in the Ito sense are given by

$$id\psi(x, t) = A\{\psi\}(x)dt + \sqrt{\frac{\gamma}{2\Delta x}}dW(x, t) \quad (8)$$

Here, $A\{\psi\}(x)$ denotes the right hand side of Eq. (1). Furthermore, $dW(x, t)$ is a complex Wiener process, meaning that the increment

$$\xi(x) = \int_{t_0}^{t_0 + \Delta t} dW(x, t). \quad (9)$$

is a complex Gaussian variable independent of t_0 , satisfying $\langle \xi(x) \rangle = 0$ and $\langle \xi(x) \xi^*(x') \rangle = \delta_{x,x'} \Delta t$. The initial conditions for this equation should be sampled from the Wigner distribution of the initial state. In the case of the vacuum, corresponding to an initially empty cavity, $\psi(x, 0)$ is also a complex Gaussian variable, such that $\langle \psi(x, 0) \rangle = 0$ and $\langle \psi(x, 0) \psi^*(x', 0) \rangle = \delta_{x,x'}/2\Delta x$. Then, the averages over this stochastic process correspond to averages over symmetrically ordered products of the field operators:

$$\langle O_1 \cdots O_N \rangle_W = \frac{1}{N!} \sum_P \left\langle \hat{O}_{P(1)} \cdots \hat{O}_{P(N)} \right\rangle. \quad (10)$$

The sum runs over all permutations of the indices P .

Usually, one is interested in normally ordered observables, which have to be symmetrized in order to be calculated from the TWM. The first order correlation is given by

$$G_1(x, x') = \left\langle \hat{\psi}^\dagger(x) \hat{\psi}(x') \right\rangle = \langle \psi^*(x) \psi(x') \rangle_W + \frac{\delta_{x,x'}}{2\Delta x}, \quad (11)$$

while the second order correlation is given by

$$\begin{aligned} G_2(x, x') &= \left\langle \hat{\psi}^\dagger(x') \hat{\psi}^\dagger(x) \hat{\psi}(x) \hat{\psi}(x') \right\rangle \\ &= \left\langle |\psi(x)|^2 |\psi(x')|^2 \right\rangle_W \\ &\quad - \frac{1 + \delta_{x,x'}}{2\Delta x} \left\langle |\psi(x)|^2 + |\psi(x')|^2 - \frac{1}{2\Delta x} \right\rangle_W \end{aligned} \quad (12)$$

The normalized second order correlation

$$g_2(x, x') = \frac{G_2(x, x')}{n(x)n(x')} \quad (13)$$

with $n(x) = G_1(x, x)$ reveal some signatures of the Hawking effect.

For the windowed Fourier transform of the field

$$\hat{\psi}_a(k, t) = \int_0^L dx e^{-ikx} w_a(x) \hat{\psi}(x, t) \quad (14)$$

the commutation relations are modified to

$$\left[\hat{\psi}_a(k), \hat{\psi}_b^\dagger(k') \right] = f_{ab}(k - k') \quad (15)$$

where

$$f_{ab}(k) = \int_0^L dx e^{-ikx} w_a(x) w_b(x). \quad (16)$$

This imposes modifications in the formulas for the momentum space correlation functions. The first order one is given by

$$\begin{aligned} G_1^{ab}(k, k') &= \langle \hat{\psi}_b^\dagger(k') \hat{\psi}_a(k) \rangle \\ &= \langle \psi_b^*(k') \psi_a(k) \rangle_W - \frac{1}{2} f_{ab}(k - k'), \end{aligned} \quad (17)$$

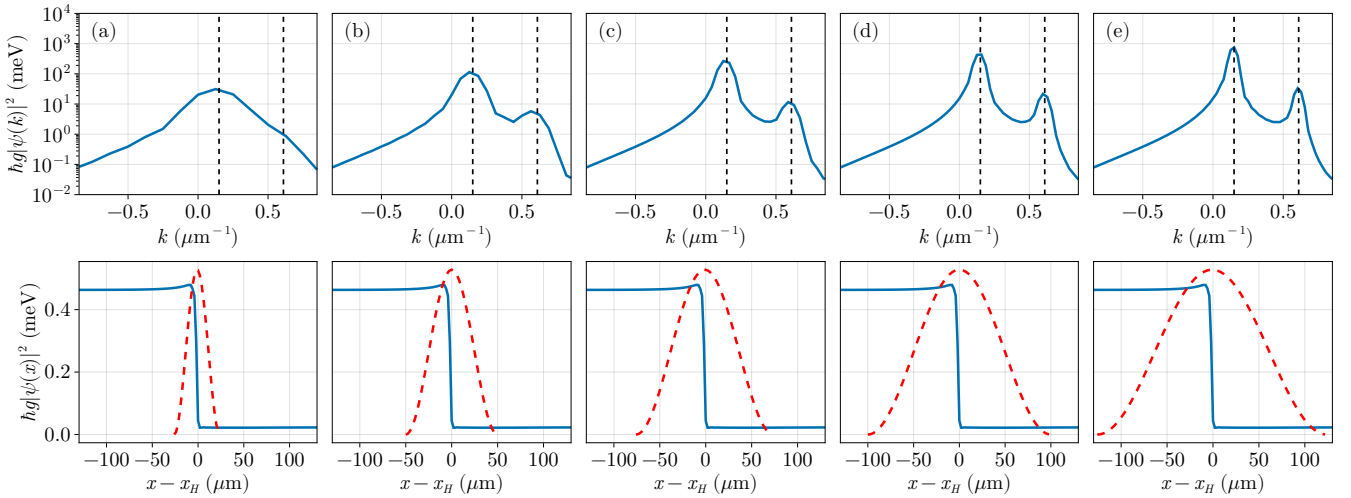


FIG. 1. Bottom row: different windows shown over the mean field position density. Top row: corresponding mean field momentum density. The windows are represented by dashed red lines. The black vertical lines correspond to the pump wavenumber k_{up} and k_{down} .

with corresponding populations $n_a(k) = G_1^{aa}(k, k)$. In an analogous manner, the second order correlation is expressed as

$$\begin{aligned}
 G_2(k, k') &= \langle \hat{\psi}_u^\dagger(k') \hat{\psi}_d^\dagger(k) \hat{\psi}_d(k) \hat{\psi}_u(k') \rangle \\
 &= \langle |\psi_u(k')|^2 |\psi_d(k)|^2 \rangle_W \\
 &\quad - \frac{1}{2} \langle |\psi_u(k')|^2 \rangle_W f_{dd}(0) \\
 &\quad - \frac{1}{2} \langle |\psi_d(k)|^2 \rangle_W f_{uu}(0) \\
 &\quad - \text{Re} [\langle \psi_u^*(k') \psi_d(k) \rangle_W f_{ud}(k - k')] \\
 &\quad + \frac{f_{uu}(0) f_{dd}(0)}{4} \\
 &\quad + \frac{|f_{ud}(k - k')|^2}{4}.
 \end{aligned} \tag{18}$$

Finally, the normalized second order correlation is given by $g_2(k, k') = G_2(k, k') / n_u(k') n_d(k)$.

CONSIDERATIONS ON WINDOW PLACEMENT

The use of a windowed Fourier transform serves many purposes in our context. From the physical point of view, by placing two windows on opposite sides of the horizon, we are able to more clearly isolate the Hawking radiation from other signals that appear in g_2 , as the strong autocorrelations, for example. Furthermore, the methods usually employed to solve the equations of motion assume periodic boundary conditions. Then, one needs to modify both the pump and the losses close to the edges in order to stably support the fluid at the desired working points, as shown in Fig. 4. These artifacts lead to the appearance of spurious signals in the momentum space correlation if one also includes the boundaries in the calculation.

However, proper use of window functions requires careful consideration of both its size and placement. The length L_w of a window defines the resolution $\Delta k_w = 2\pi/L_w$ in momentum space that can be resolved. This is a reflex of the uncertainty relation between Fourier pairs. Therefore, a localized window gives poor momentum resolution. To illustrate this point, we show, in Fig. 1, the momentum density $|\psi(k)|^2$ for different window lengths, all centered at the horizon. As both the upstream and downstream regions fall under the window, we should see two peaks corresponding to k_{up} and k_{down} . Although they are clearly visible in 1(e), when the window is large, they become less pronounced until they merge completely in 1(a). This spread of the peaks is a manifestation of spectral leakage.

In order to eliminate autocorrelation signals in g_2 , one would like to place windows completely contained on different sides of the horizon, as shown in Fig. 2(a,e). However, this placement only leaves us with the sharp population peaks corresponding to the pump. This is due to the dissipative nature of the polaritons, which causes the other momentum components created at

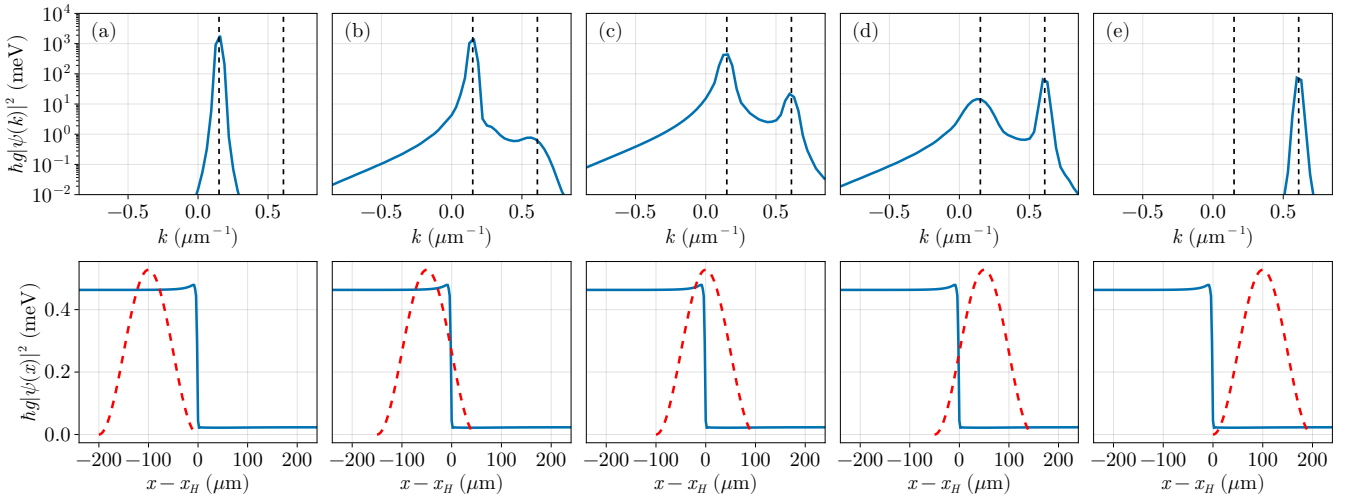


FIG. 2. Bottom row: different windows shown over the mean field position density. Top row: corresponding mean field momentum density. The windows are represented by dashed red lines. The black vertical lines correspond to the pump wavenumber k_{up} and k_{down} .

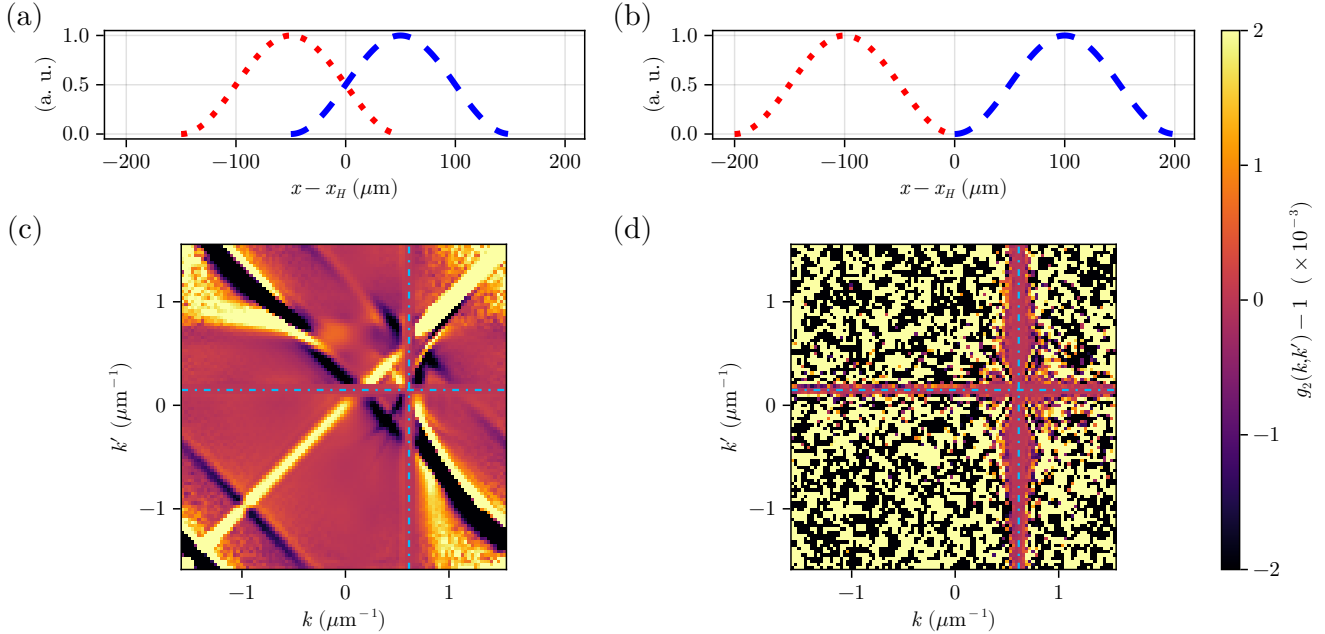


FIG. 3. (a) and (b) correspond to the pairs of windows that generate the momentum density correlations in (c) and (d), respectively. In this simulation, 1.7×10^8 realizations were performed.

the horizon to leave the cavity before reaching the maximum of the window. In this case, we would not be able to observe the Hawking effect, as there would be no population in the required modes. As discussed above, one also cannot use small windows, as that would cause a severe spectral leakage. The best compromise, as employed in the main text, is to place the windows only partially in each region, as in Fig. 2(b,d). This ensures a sufficient momentum resolution, a significant damping of the autocorrelations, while also allowing for the Hawking radiation to reach the maximum of the window before leaving the cavity.

To further illustrate this point, we show, in Fig. 3, the value of g_2 for two more different pairs of windows. One can see that, when the windows are fully contained within each region, as shown in (b), the corresponding momentum correlations in (d) display only noise, which is consistent with an extremely low occupation number of the corresponding wavevectors.

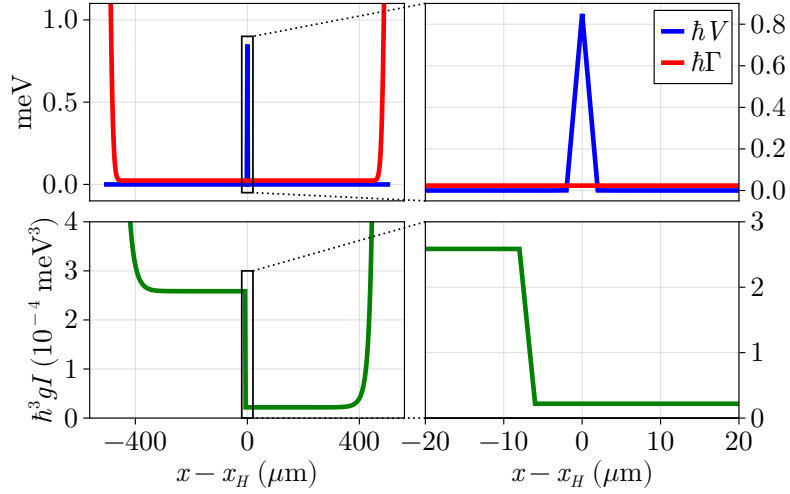


FIG. 4. Top row: potential and losses; bottom row: intensity profile.

STABILIZATION OF THE FLUID IN THE NUMERICAL SIMULATION

Due to the fact that we are working very close to the critical point of the bistability cycle, it is hard, both numerically and experimentally, to stabilize the polariton fluid in the desired working point. This is further complicated in the numerical case, as the utilized algorithm assumes periodic boundary conditions. In this section we describe the prescription used to achieve a flat and stable configuration of the fluid in both the upstream and downstream regions.

First, to avoid undesired effects arising from the periodic boundary conditions, we use a modified spatially dependent loss

$$\Gamma(x) = \gamma + \gamma_{damp}[G(x; 0, w_{damp}) + G(x; L, w_{damp})] \quad (19)$$

which rises significantly close to the edges of the simulated cavity. In the above equation, G denotes a Gaussian function: $G(x; x_0, w) = e^{-(x-x_0)^2/w^2}$.

The pump is also modified to rise in the edges, up to a value F_M :

$$F(x, t) = \begin{cases} [F_{up} + (F_M - F_{up}) \operatorname{sech}(x/w_p)] e^{ik_{up}x - \omega_p t} h(t), & x < x_s \\ [F_{down} + (F_M - F_{down}) \operatorname{sech}((x-L)/w_p)] e^{ik_{down}x - \omega_p t} h(t), & x > x_s \end{cases} \quad (20)$$

Here, x_s is the position of the step of the pump. Furthermore,

$$h(t) = 1 + A e^{-t/\tau} \quad (21)$$

is a term representing an extra amplitude A at the start of the pumping scheme in order to rise the fluid to the top of the bistability curve. This term decays after a transient time τ .

We also included a potential $V(x) = V_0 G(x; x_d, w_V)$ localized around the position x_d .

All of these terms are illustrated in Fig. 4

NUMERICAL PARAMETERS

In table I, we display the numerical values of all the relevant parameters that were used in the simulations presented in this work.

FROM MOMENTUM-SPACE $g^{(2)}$ TO PHOTOCURRENT CORRELATIONS

Let the total optical power collected from window $a \in \{u, d\}$ be P_a . The mean photo-electron rate on detector a is

$$R_a = \eta_a \mathcal{T}_a \frac{P_a}{\hbar \omega_0}, \quad (22)$$

Parameter name	Parameter symbol	Parameter value
Cavity length	L	$1024 \mu\text{m}$
Number of points in the grid	N	512
Grid spacing	Δx	$2 \mu\text{m}$
Time step of the simulation	Δt	0.2 ps
Simulation duration	T	400 ps
Number of realizations	N_{sim}	5.5×10^8
Planck's constant	\hbar	$0.6582 \text{ meV} \cdot \text{ps}$
Loss	γ	$0.047 \text{ meV}/\hbar$
Polariton mass	m^*	$1/6 \text{ meV} \cdot \text{ps}^2 \cdot \mu\text{m}^{-2}$ ^a
Detuning	$\delta(0)$	$0.49 \text{ meV}/\hbar$
Nonlinear constant	g	$3 \times 10^{-4} \text{ meV} \cdot \mu\text{m}/\hbar$
Extra damping at the edges	γ_{damp}	$4.5 \text{ meV}/\hbar$
Width of the damping at the edges	w_{damp}	$20 \mu\text{m}$
Upstream pump momentum	k_{up}	$0.148 \mu\text{m}^{-1}$
Downstream pump momentum	k_{down}	$0.614 \mu\text{m}^{-1}$
Upstream pump amplitude	F_{up}	$1.410 \text{ ps}^{-1} \cdot \mu\text{m}^{-1/2}$
Downstream pump amplitude	F_{down}	$0.410 \text{ ps}^{-1} \cdot \mu\text{m}^{-1/2}$
Maximum pump amplitude	F_{M}	$20 \text{ ps}^{-1} \cdot \mu\text{m}^{-1/2}$
Width of the pump at the edge	w_{p}	$20 \mu\text{m}$
Position of the potential step	x_{s}	$505 \mu\text{m}$
Extra amplitude factor	A	6
Transient time	τ	50 ps
Position of the deffect	x_{d}	$512 \mu\text{m}$
Potential amplitude	V_0	$0.85 \text{ meV}/\hbar$
Width of the potential	w_{V}	$0.75 \mu\text{m}$

^aThis is roughly 3×10^{-5} the mass of the electron

TABLE I. Numerical values of the parameters relevant to the simulation.

with overall quantum efficiency η_a and optical throughput \mathcal{T}_a . The normally ordered, time-resolved cross-correlation of the photocurrents is

$$C_{ud}(\tau) \equiv \langle : \delta i_u(t) \delta i_d(t + \tau) : \rangle = e^2 R_u R_d [g_{ud}^{(2)}(\tau) - 1], \quad (23)$$

where $g_{ud}^{(2)}(\tau)$ is the *time-domain* second-order correlation integrated over the momentum windows defined by $w_{u,d}$.

In continuous-wave operation with sampling bin Δt comparable to the correlation time τ_c (set by the polariton lifetime and detection bandwidth), the expected number of coincidences accumulated over a total integration time T is

$$N_{\text{acc}} = R_u R_d \Delta t T, \quad N_{\text{true}} = R_{\text{pair}} T, \quad (24)$$

and the measured zero-delay correlation is

$$g_{ud}^{(2)}(0) \simeq 1 + \frac{N_{\text{true}}}{N_{\text{acc}}} = 1 + \frac{R_{\text{pair}}}{R_u R_d \Delta t}. \quad (25)$$

Comparing with the definition used in the main text at equal times,

$$\delta g^{(2)} \equiv g_{ud}^{(2)}(0) - 1, \quad (26)$$

we identify the pair rate into the two detected momentum windows as

$$R_{\text{pair}} = \delta g^{(2)} R_u R_d \tau_c, \quad (\Delta t \sim \tau_c). \quad (27)$$

Equation (27) allows to interpret the numerically obtained $\delta g^{(2)}$ as an excess coincidence probability per correlation time (not a fractional increase of the singles rate). Note that the dependence is quadratic in the singles and linear in the correlation time.

When $\delta g^{(2)} \ll 1$ (our case), accidental coincidences dominate the variance, giving

$$\text{SNR} \simeq \frac{N_{\text{true}}}{\sqrt{N_{\text{acc}}}} = \delta g^{(2)} \sqrt{R_u R_d \tau_c T}. \quad (28)$$

To reach a significance s one needs

$$T \simeq \frac{s^2}{[\delta g^{(2)}]^2 R_u R_d \tau_c}. \quad (29)$$

For illustration: if each arm carries $R_u = R_d = 10^8 \text{ s}^{-1}$ (easily obtained after attenuation from $P_a \sim 0.1 \mu\text{W}$ at near-IR frequencies with Si or InGaAs photodiodes operated linearly), $\tau_c \sim 10 \text{ ps}$, and $\delta g^{(2)} \sim 10^{-3}$, then $R_u R_d \tau_c \simeq 10^5$ and a 5σ detection requires $T \simeq 25/(10^{-6} \times 10^5) \approx 250 \text{ s}$, that is, about four minutes.

Balanced detection is used to suppress classical common-mode noise from the pump. Practically, each momentum window is split 50:50; one output goes to the “signal” photodiode and the other to a reference diode. The two currents of each pair are subtracted (with appropriate gain balancing), producing shot-noise-limited residuals \tilde{i}_u, \tilde{i}_d . The Hawking signal is obtained from the cross-correlation $\langle \tilde{i}_u(t) \tilde{i}_d(t + \tau) \rangle$. Because the subtraction is local to each arm, the mean singles rates in Eq. (29) must be understood as the post-split rates; the improvement comes from removing classical intensity noise without affecting the normally ordered cross-correlation, which is preserved by passive linear optics.

Alternatively, one may estimate the zero-frequency cross-spectrum $S_{ud}(0) = 2e^2 R_u R_d \int d\tau [g_{ud}^{(2)}(\tau) - 1]$, using RF spectrum analyzers with bandwidth B . The integrated SNR then scales as $\propto \delta g^{(2)} \sqrt{R_u R_d \tau_c T}$, identical to Eq. (29). Fast time resolution is unnecessary, provided that the electronics bandwidth exceeds $1/\tau_c$.

* maxime.jacquet@lkb.upmc.fr

[1] I. Carusotto and C. Ciuti, Quantum fluids of light, *Reviews of Modern Physics* **85**, 299 (2013).
[2] I. Carusotto and C. Ciuti, Spontaneous microcavity-polariton coherence across the parametric threshold: Quantum monte carlo studies, *Phys. Rev. B* **72**, 125335 (2005).